# Anisotropy in the salt outcrop at Cardona, Catalonia – implications for seismic imaging

**Martin Landrø,[1*] Cai Puigdefabregas[1] and Børge Arntsen[1]**

## Abstract

The world's largest oil discoveries in recent years have been pre-salt, in reservoirs located below or close to salt bodies. It is often assumed that the salt is homogeneous and that a near-constant isotropic velocity in the salt body can be used for seismic imaging. Here we show that this simplification may be too simple. Based on field observations from an old salt mine in Spain, we estimate anisotropic parameters describing the exploited salt diapir. In its outcrop we identify a regular pattern of alternating halite and clay layers, where the thickness of each layer is close to periodic. From this observation, we estimate corresponding anisotropic parameters for this salt outcrop and find that the degree of anisotropy is moderate, of the order of 5% difference between horizontal and vertical velocities. Furthermore, we identify potential shear zones within the salt outcrop that can be mapped over distances of several hundred metres. The thicknesses of these shear zones are of the order of metres. Based on these observations, it is a huge simplification to treat salt bodies as homogeneous and isotropic for seismic imaging purposes.

## Introduction

Creating seismic images of sedimentary structures beneath salt is commonly extremely challenging due to the complicated geometrical shapes of salt bodies (Pan et al., 2006; Mitchell et al., 2007). For imaging purposes, salt bodies are conventionally assumed to be homogeneous with no internal structure, but it is known that salt in some areas has large-scale internal layering (Huang et al., 2010). Ji et al. (2010) showed that subsalt structures could be better imaged by using velocity fields with vertical variation in salt bodies, and Bowling et al. (2010) found that considerable improvement in subsalt image quality could be achieved by including velocity anisotropy in sediments around salt bodies. It is, therefore, reasonable to suggest that taking internal salt anisotropy into account could further boost subsalt image quality.

In May 2009, we visited the Cardona salt mine in Spain (Figure 1). A geological map and cross-sections are shown in Figures 2 and 3. Cardona supplied Catalonia with salt for several centuries, ensuring a strong economy for this city. When mining ended some 20 years ago, the salt was being produced from approximately 1000 m depth. Today, there is no production from this salt mine, but it is open for tourists to visit.

The Cardona diapir is an elongated anticline with a salt core formed ahead of the Pyrenean thrust system with subsequent diapirism. A section through the basin from the Pyrenees to the foreland (Figures 2 and 3) shows the position of the Cardona diapir between the active Pyrenean thrusting to the north and the more passive foreland margin to the south, represented by the Montserrat alluvial fan conglomerate.

***Figure 1*** *The Cardona salt diapir outcropping just behind the large body of salt dump. To the right, part of the town of Cardona, is the ancient shaft and the entrance for visitors. The salt is flanked by reddish lacustrine-fluviatile sequences, and capped by brownish Quaternary sediments.*

The sedimentary succession, Upper Eocene to Oligocene in age, was deposited when the basin lost connection to the Atlantic Ocean because of Pyrenean tectonics. The basin became confined and evaporites deposited (gypsum, halite, carnallite, and sylvite) over the Upper Eocene marine sequence. During the Late Eocene, a lacustrine sequence was deposited over the salt and finally a thick Oligocene fluvial and lacustrine succession filled up the basin.

## Thin clay layers embedded in salt

Inside the salt mine thin clay layers may be observed, embedded in the halite (Figures 4–6). In some areas, the laminar clay layers are planar and parallel (Figure 4), and in other areas

[1] *NTNU (Norwegian University of Science and Technology), 7491 Trondheim, Norway.*
* *Corresponding author, E-mail: martin.landro@ntnu.no*

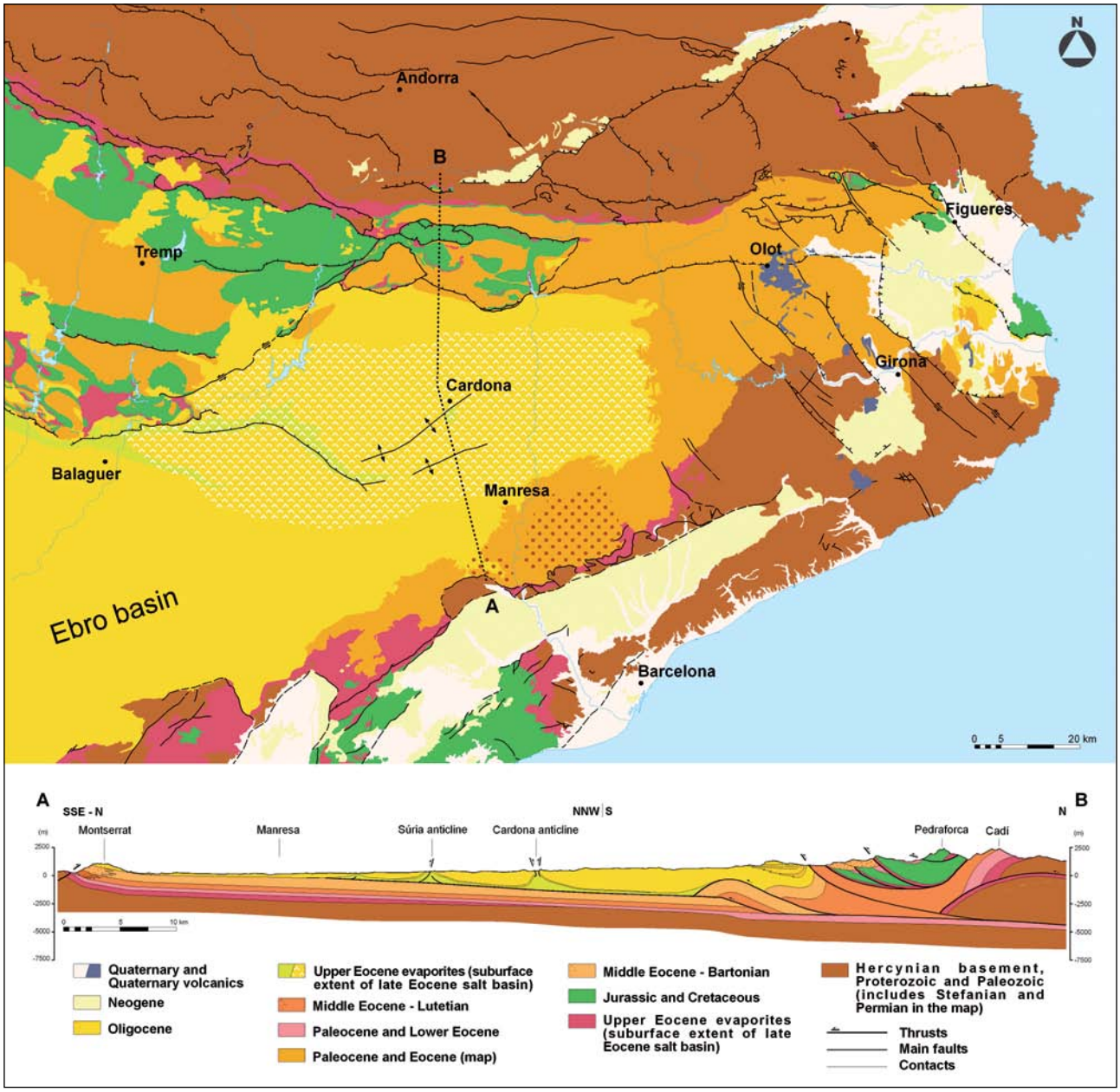


***Figure 2*** *Geological map and cross-section showing the location of the Cardona diapir. Notice the salt-cored anticlines in relation to the development of the Pyrenean thrust system (modified from Munoz and Martinez, 2010).*

they are strongly folded (Figures 5 and 6). As a first attempt, we will use the first example as input to our seismic analysis.

It is well known that a periodic medium like the one shown in Figure 4 will be anisotropic (e.g., Backus, 1962; Folstad and Schoenberg, 1992; Stovas et al., 2006). The basic idea (Backus, 1962) is that if the seismic wavelength is significantly larger than the thickness of individual layers, it is possible to model the finely layered medium as an anisotropic medium. Thus an inhomogeneous medium with a huge number of layers may be treated as one thick anisotropic layer, known as the effective medium. In this context, anisotropy means that the seismic velocity varies with propagation direction. In our example, it means that we have to estimate anisotropy parameters representing the layered salt body. For simplicity, and based on the observations in the mine, we estimate seismic anisotropy parameters for a periodic binary medium (i.e., two components only) consisting of clay and halite.

Let us denote clay as component 1 and halite as component 2, with symbols $\alpha$, $\beta$ and $\rho$ denoting P-wave velocity, S-wave velocity and density, respectively. Let $\kappa$ denote the net to gross ratio (thickness of clay divided by total thickness of halite and clay), expressed as a fraction between zero and one. The seismic parameters used for the two components are listed in Table 1. Thomsen (1986) introduced a set of parameters that can be used to describe an anisotropic medium. The fractional amount by which the horizontal P-wave velocity in

| | P-wave velocity (m s$^{-1}$) | S-wave velocity (m s$^{-1}$) | Density (kg m$^{-3}$) |
|---|---|---|---|
| Clay (component 1) | 2500 | 1000 | 2300 |
| Halite (component 2) | 4500 | 2500 | 2100 |

***Table 1*** *Seismic parameters for clay and halite used in the anisotropic analysis.*

the effective medium exceeds the vertical P-wave velocity is given by the anisotropy parameter (Stovas et al., 2006):

$$\varepsilon = 2\gamma_1^2 \kappa(1-\kappa)\Delta c_{44}\Delta_1, \tag{1}$$

where

$$\gamma_1 = \beta_1 / \alpha_1,$$

$$\Delta_1 = \frac{\Delta c_{33}(1-\frac{1}{2}\Delta c_{44}) - \gamma_1^2 \Delta c_{44}(1-\frac{1}{2}\Delta c_{33})}{(1-\frac{1}{2}\Delta c_{44})^2(1+\frac{1}{2}\Delta c_{33})},$$

$$\Delta c_{33} = 2\frac{c_{33,2}-c_{33,1}}{c_{33,2}+c_{33,1}}, \quad \Delta c_{44} = 2\frac{c_{44,2}-c_{44,1}}{c_{44,2}+c_{44,1}},$$

$$c_{33,1} = \alpha_1^2\rho_1,\ c_{33,2} = \alpha_2^2\rho_2,\ c_{44,1} = \beta_1^2\rho_1, \text{ and } c_{44,2} = \beta_2^2\rho_2.$$

Figure 7 shows $\varepsilon$ as a function of net to gross assuming an S-wave velocity in clay of 1000 m s$^{-1}$ and 1500 m s$^{-1}$. Figure 8 shows the ratio between the horizontal and vertical P-wave velocity versus net to gross.

The P-wave velocity for weak anisotropy is given as (Thomsen, 1986):

$$\alpha(\theta) = \alpha_V(1+\delta\sin^2\theta\cos^2\theta+\varepsilon\sin^4\theta), \tag{2}$$

where $\theta$ is the angle between the wavefront normal and the normal to the bedding. The relative P-wave velocity as a function of $\theta$ is shown in Figure 9, assuming 10% clay within the halite.

## Shear wave anisotropy

The anisotropy parameter $\delta$ introduced by Thomsen (1986) is

$$\delta = \frac{(c_{13}+c_{44})^2-(c_{33}-c_{44})^2}{2c_{33}(c_{33}-c_{44})}, \tag{3}$$

where (Stovas et al., 2006)

$$c_{13} = c_{33,1}\frac{1-2\gamma_1^2+\frac{2\gamma_1^2(\Delta c_{33}-\Delta c_{44})}{(1-\frac{1}{2}\Delta c_{44})(1+\frac{1}{2}\Delta c_{33})}}{1-\frac{\kappa\Delta c_{33}}{1+\frac{1}{2}\Delta c_{33}}},$$

$$c_{33} = c_{33,1}\frac{1}{1-\frac{\kappa\Delta c_{33}}{1+\frac{1}{2}\Delta c_{33}}} \text{ and } c_{44} = c_{44,1}\frac{1}{1-\frac{\kappa\Delta c_{44}}{1+\frac{1}{2}\Delta c_{44}}}$$

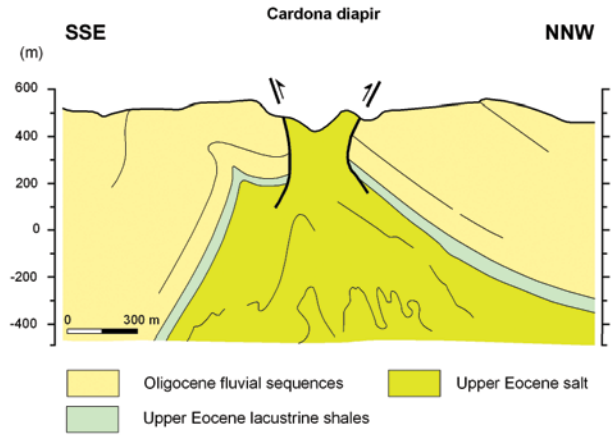


***Figure 3*** *Detailed section of the Cardona salt diapir (modified from Munoz and Martinez, 2010).*

***Figure 4*** *Thin clay layers (dark grey) embedded in the halite (white and red).*

***Figure 5*** *Folding of salt layers in the Cardona salt mine.*

***Figure 6*** *The banded pattern corresponds to halite cycles that include a thin layer of clay (dark grey, about 1 mm thick), and a layer of white, light grey, or iron-stained orange-reddish halite (average 4 mm thick). The field of view pictured is a couple of metres wide.*

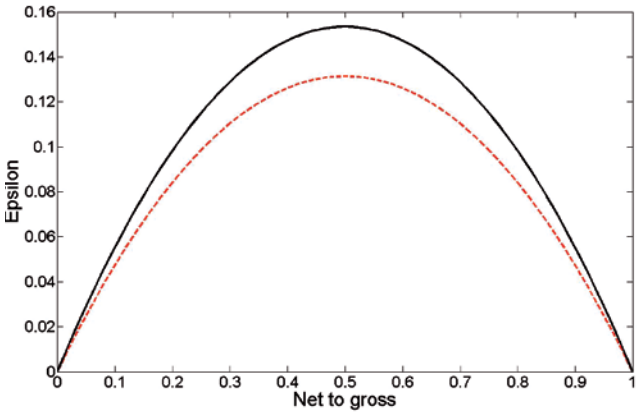


*Figure 7* Anisotropy parameter $\varepsilon$ (epsilon) as a function of net to gross for S-wave velocity in clay of 1000 m s$^{-1}$ (black solid line) and 1500 m s$^{-1}$ (red dashed line).

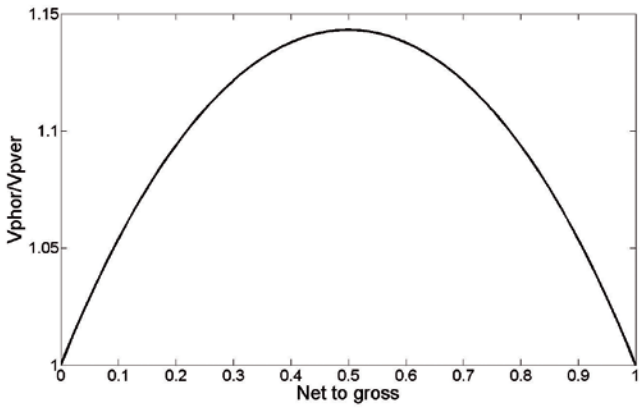


*Figure 8* Ratio of horizontal (i.e., bedding-parallel) to vertical P-wave velocity in a periodic halite-clay medium as a function of net to gross.

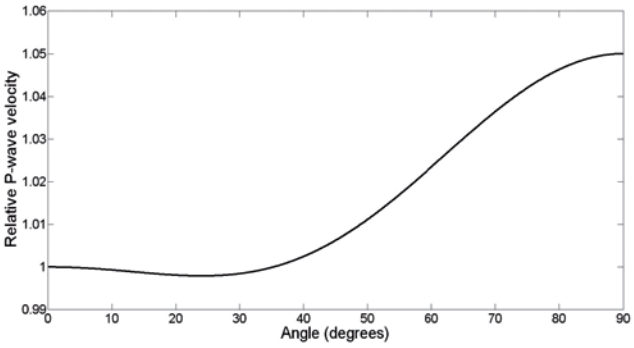


*Figure 9* P-wave velocity versus $\theta$ assuming 10% clay within the halite for $\varepsilon$ = 0.05 and $\alpha$ = –0.025.

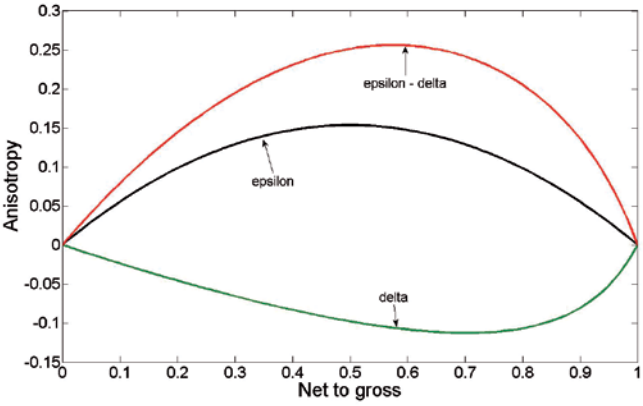


*Figure 10* Anisotropy parameters $\varepsilon$ (epsilon), $\delta$ (delta) and their difference as functions of net to gross.

Figure 10 shows $\varepsilon$ and $\delta$ as functions of net to gross ratio. The S-wave velocity for the SV-mode is given as a function of angle $\theta$ as (Thomsen, 1986):

$$\beta(\theta) = \beta_v \left[ 1 + (\varepsilon - \delta) \frac{\alpha_v^2}{\beta_v^2} \sin^2 \theta \cos^2 \theta \right]. \quad (4)$$

Assuming a net to gross of 10%, $\varepsilon - \delta = 0.08$. Using this value in Equation (4) gives a shear wave (SV mode) velocity variation as shown in Figure 11. For simplicity, we have assumed that the vertical P-wave and S-wave velocities are equal to the values for salt given in Table 1.

## Shear zones within the salt

Figure 12 is a photograph from inside the salt mine which shows the transition from a laminar pattern via folding to a more chaotic zone which we interpret as a shear zone. The width of this shear zone is 1–2 m, and the central part of it is recrystallized in some areas. Figure 13 is a photograph of the salt outcrop outside the mine, and the possible location of the shear zone has been interpreted on this picture. Such shear zones, which may be several metres thick, could introduce velocity variations within a salt body that influence the quality of seismic imaging. An outstanding question is whether these shear zones are created by the presence of the clay, or whether they can also exist in apparently homogeneous halite. This issue requires further investigation.

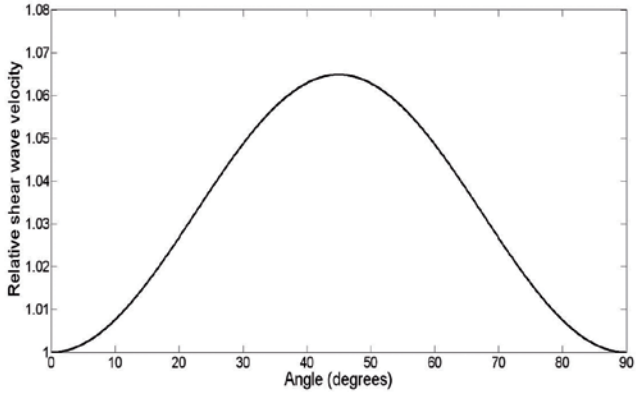


*Figure 11* S-wave velocity (SV mode) versus $\theta$ for a net to gross of 10% (10% clay within the halite).

## Discussion and conclusions

The presence of clay in a salt diapir leads to anisotropic seismic properties. Based on field observations from the Cardona salt mine, we estimate that for this particular salt diapir the anisotropy is moderate, but not negligible. Assuming the clay to halite ratio is 10%, the difference in

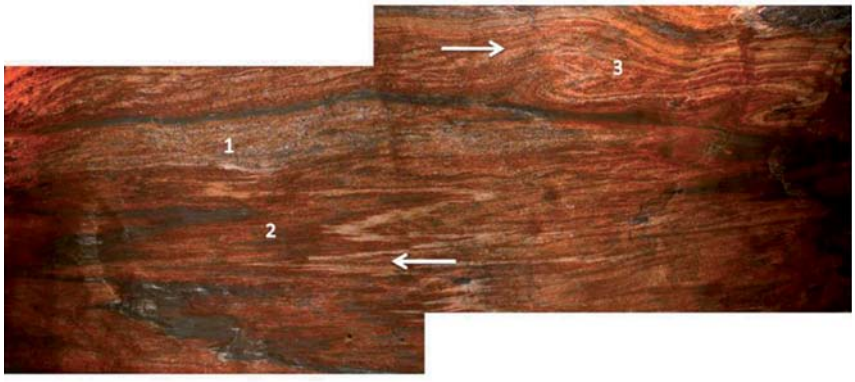


***Figure 12*** *A wide shear zone seen on the gallery ceiling (about 2 m between the white arrows). The recrystallized band labelled 1 is about 50 cm wide and corresponds to the most sheared zone. Tight folding labelled 2 appears to be affected by shear planes. Folding labelled 3 indicates sense of shear, interpreted as indicated by the white arrows.*

***Figure 13*** *Trace of the shear zone (red line) at outcrop, probably corresponding to the shear zone in the mine gallery (Figure 12).*

P-wave velocities parallel and perpendicular to the bedding is 5%. Such anisotropic velocity variations may be important to include in seismic migration, and may lead to improved definition of the salt body.

Furthermore, the presence of clay within salt may change the plastic behaviour of the salt and introduce shear zones within the salt. Such phenomena may create velocity heterogeneities on a larger scale than the clay-halite layering discussed above. Based on observations from the salt in Cardona, it is obvious that it is a huge simplification to treat salt as a homogeneous body with a constant velocity.

## Acknowledgements

We thank Statoil for financial support, and especially Bjørn Rasmussen and Ragnar Knarud for initiating the field course in the Pyrenees. We are also indebted to Josep Munoz for discussions and for introducing us to the Cardona salt mine. We also thank the Norwegian Research Council for financial support to the ROSE (Rock Seismic) consortium at NTNU, and the reviewer for constructive comments.

## References

Backus, G.E. [1962] Long-wave elastic anisotropy produced by horizontal layering. *Journal of Geophysical Research*, **67**, 4427–4440.

Bowling, J., Ji, S., Lin, D., Chergotis, D., Nolte, B. and Yanchak, D. [2010] Mad dog TTI RTM: better than expected. *80th SEG Annual Meeting*, Expanded Abstracts, **29**, 3313–3317.

Brown, R.J. and Sun, Z. [1993] An underground seismic-anisotropy experiment in a salt mine. *Crewes Research Report*, **5**(4).

Folstad, P.G. and Schoenberg, M. [1992] Low frequency propagation through fine layering. *62nd SEG Annual Meeting*, Expanded Abstracts, **11**, 1278–1281.

Huang, Y., Lin, D., Bai, B., Roby, S. and Ricardez, C. [2010] Challenges in presalt depth imaging of the deepwater Santos Basin, Brazil. *The Leading Edge*, **29**, 820–825.

Ji, S., Huang, T., Fu, K. and Li, Z. [2010] Dirty salt velocity inversion: the road to a clearer subsalt image. *80th SEG Annual Meeting*, Expanded Abstracts, **29**, 4103–4107.

Mitchell, S., Sharp, J. and Chergotis, D. [2007] Dual-azimuth versus wide-azimuth technology as applied in subsalt imaging of Mad Dog Field – a case study. *The Leading Edge*, **26**, 470–478.

Pan, J., Barnes, B., Kong, F., Chang, M., Kriechbaum, V., Li, Z., Rodriguez, G., Zhang, L., Chang, I. and Chen-Bin, S. [2006] Depth imaging and regional exploration in Northeast Garden Banks, Gulf of Mexico. *The Leading Edge*, **25**, 468–473.

Munoz, J. and Martinez, A. [2010] In: *Atles Geològic de Catalunya*. Institut Cartogràfic de Catalunya, Barcelona, 136–137.

Stovas, A., Landrø, M. and Avseth, P. [2006] AVO attribute inversion for finely layered reservoirs. *Geophysics*, **71**, C25–C36.

Thomsen, L. [1986] Weak elastic anisotropy. *Geophysics*, **51**, 1954–1966.

*Received 31 January 2011; accepted 16 May 2011.*
doi: 10.3997/1365-2397.2011022